FULL PAPER

ADVANCED
OPTICAL
MATERIALS

www.advopticalmat.d

Check for
updates

Flexible Near-Infrared InGaSb Nanowire Array Detectors with Ultrafast Photoconductive Response Below 20 μs

*Dapan Li, SenPo Yip, Fangzhou Li, Heng Zhang, You Meng, Xiuming Bu, Xiaolin Kang, Changyong Lan, Chuntai Liu, and Johnny C. Ho**

High-performance flexible room-temperature near-infrared (NIR) photodetectors are one of the important components for image sensing, data communication, environmental monitoring, and bioimaging applications. However, there is still a lack of suitable device channel materials to provide high sensitivity as well as good mechanical flexibility for photodetection, particularly operating at the optical communication wavelength of 1550 nm. In this work, highly crystalline $In_{0.28}Ga_{0.72}Sb$ nanowires (NWs) are successfully grown by the two-step chemical vapor deposition method and assembled into high-density regular NW parallel arrays on polyimide substrates. When they are constructed into photodetectors without using any p–n junctions, they exhibit the excellent responsivity up to 1520 A W^{-1} and ultra-fast response speed below 20 μs toward 1550 nm irradiation at room temperature, which constitutes a record high performance among all flexible NIR photodetectors reported in recent literature. Notably, these flexible NW parallel-array photodetectors also display a superior mechanical flexibility and operation durability. They not only provide a stable photoresponse under illumination on–off cycles up to 1000 s, but also maintain the steady photocurrent without any significant degradation after 700 bending cycles. All these results evidently indicate the promising potential of these crystalline $In_{0.28}Ga_{0.72}Sb$ NW parallel arrays for next-generation flexible optoelectronic devices.

1. Introduction

In the past decade, flexible electronics have attracted a tremendous amount of research and development interests.[1,2] They not only enable many unique device properties that cannot be achieved by conventional electronics, but also open up promising directions for flexible solar cells,[3] wearable diagnostic systems,[1,2] stretchable electronic skins,[4,5] flexible photodetectors,[6] and many others.[1,7] Among these new device concepts, flexible photodetectors hold paramount importance for future applications, such as building on-skin medical diagnostics, artificial visual systems, and biological signal monitoring. These applications are believed to ultimately change our lifestyle as well as improve our life quality.[3,8,9]

Generally, flexible photodetectors have been constructed based on different crystalline nanoscale materials as device channels,[10] which include 1D and 2D nanostructures because of their excellent optoelectronic properties and mechanical flexibility as compared with the typical thin film counterparts. In fact, apart from the flexibility, 1D nanowire (NW) materials also have superior surface-to-volume ratio that would contribute to the enhanced carrier separation and collection when they are configured into photodetectors. In this manner, combined with their high carrier mobility and appropriate direct band gap, III–V compound semiconductor NWs are always put together as fundamental building blocks for next-generation high-performance electronics,[11] optoelectronics,[12,13] and energy harvesting applications.[14] Until now, there have been numerous reports focused on III–V NW-based photodetectors constructed on rigid substrates, exhibiting high sensitivity and fast responsivity.[15–19] However, to the best of our knowledge, there are very limited works on flexible photodetectors utilizing III–V NWs, especially for the

Dr. D. Li, Dr. S. P. Yip, F. Li, H. Zhang, Y. Meng, X. Bu, X. Kang, Prof. J. C. Ho
Department of Materials Science and Engineering
City University of Hong Kong
Kowloon, Hong Kong SAR 999077, China
E-mail: Johnnyho@cityu.edu.hk
Dr. S. P. Yip, H. Zhang, Prof. J. C. Ho
State Key Laboratory of Terahertz and Millimeter Waves
City University of Hong Kong
Kowloon, Hong Kong SAR 999077, China

Dr. S. P. Yip, Prof. J. C. Ho
Shenzhen Research Institute
City University of Hong Kong
Shenzhen 518057, China
Dr. C. Lan
State Key Laboratory of Electronic Thin Films and Integrated Devices
School of Optoelectronic Science and Engineering
University of Electronic Science and Technology of China
Chengdu 610054, China
Prof. C. Liu
Key Laboratory of Advanced Materials Processing & Mold
(Zhengzhou University)
Ministry of Education
Zhengzhou University
Zhengzhou 450002, China

near-infrared (NIR) region, which has important utilization in the optical communication band (1260 to 1625 nm) with low-loss data transmission.[20]

For the optical communication band, antimonide-based NWs are widely exploited as active materials for optoelectronic devices due to their high carrier mobility and small direct band gap.[19,21–24] For instance, Ma et al. fabricated individual NW photodetectors on silicon using GaSb/GaInSb p–n heterojunction NW channels, where the devices were capable of operating at room temperature, exhibiting high external quantum efficiency of 10^4, high responsivity of 10^3 A W^{-1} and short response time of 2 ms under the illumination of 1550 nm light.[19] Nevertheless, these complicated NW heterojunctions may not be favorable and applicable for large-scale device integration. Lately, high density, crystalline and phase-pure In$_x$Ga$_{1-x}$Sb NWs were successfully grown by two-step chemical vapor deposition (CVD), in which the precursor powder mixture ratio of InSb and GaSb could be well-controlled to reliably vary the chemical composition of obtained NWs with x up to 0.28.[22] When configured into simple NIR photodetectors based on individual In$_x$Ga$_{1-x}$Sb on rigid substrates, they even delivered better device characteristics as compared with the GaSb/GaInSb p–n heterojunction devices.

Here, we further extend these highly-crystalline In$_x$Ga$_{1-x}$Sb NWs into large-scale uniform parallel arrays on plastics for the efficient, room temperature and mechanically flexible NIR photodetectors. To be specific, In$_{0.28}$Ga$_{0.72}$Sb NWs are selected to be the device channel material as they yield the best photoresponse among all the different NW compositions, attributable to the reduced band gap and enhanced absorption coefficient toward 1550 nm irradiation. Once these NWs are assembled into high-density and well-aligned parallel arrays on polyimide (PI) substrates, they can be fabricated into flexible NIR photodetectors, demonstrating the excellent responsivity up to 1520 A W^{-1} and ultra-fast response speeds (i.e., rise and decay time constants) below 20 µs at room temperature. Without using any p–n junctions, this efficient photoresponse can be regarded as a record among all the flexible NIR detectors. More importantly, these flexible devices exhibit robust mechanical stability during the bending test. After 700 bending cycles, there is only a slight degradation of 7% observed in the device's photocurrent. All these results can evidently indicate the promising potential of In$_x$Ga$_{1-x}$Sb NWs for high-performance flexible optoelectronic devices.

2. Results and Discussion

In this work, the non-epitaxial growth of In$_{0.28}$Ga$_{0.72}$Sb NWs was readily achieved by the two-step CVD method.[22] As shown in the SEM image in **Figure 1**a, the obtained NWs have a high growth density, with a uniform and smooth morphology, grown on amorphous Si/SiO$_2$ substrates. Based on the detailed TEM analysis, the length of NWs is greater than 10 µm with an average diameter of 57 ± 10 nm (Figure S1, Supporting Information). It is also observed that the typical NW consists of a hemispherical catalytic tip (Figure 1b), which indicates the vapor-liquid-solid growth mechanism of In$_{0.28}$Ga$_{0.72}$Sb NWs, being consistent with the previous report. Moreover, energy
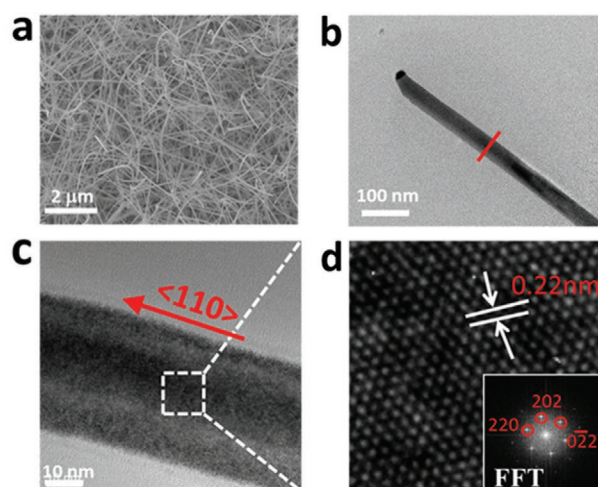

Figure 1. a) SEM image of the grown In$_{0.28}$Ga$_{0.72}$Sb NWs. b) TEM image of a typical In$_{0.28}$Ga$_{0.72}$Sb NW showing the catalytic tip. c,d) HRTEM image and corresponding lattice fringes indicating the crystallinity and interplanar spacing of the NW. Inset shows the FFT pattern verifying the growth orientation along <110> direction and excellent crystallinity.

dispersive X-ray spectroscopy is performed to confirm the NW composition (Figure S2, Supporting Information), whereas the corresponding line scan is carried out on the NW radial direction to assess the composition uniformity (Figure S3, Supporting Information). Importantly, the NW body has a uniform diameter along the axial direction without any evidence of the tapering (Figure 1c). Almost all of the NWs are determined to have a growth orientation of <110> as well as an excellent crystallinity without any noticeable planar defects. There are clear lattice fringes with the interplanar distance of 2.2 Å, which corresponds to the spacing along {110} planes of the In$_{0.28}$Ga$_{0.72}$Sb NWs (Figure 1d).[22] These phase- and orientation-pure NWs with minimized defect concentrations would lead to reduced charge carrier scattering that is essential for high-performance electronic and optoelectronic applications.

Once the high-quality In$_{0.28}$Ga$_{0.72}$Sb NWs are successfully grown, they can be assembled into large-scale regular NW parallel arrays on PI substrates by contact printing.[25–27] To be specific, photolithography is utilized to define the location of NW printing regions. This patterning ability is advantageous for the fabrication of large-scale device arrays for further system integration in future.[25,27] As depicted in the dark-field optical image in **Figure 2**a, the patterns of NW parallel-array thin films with the dimension of 250 µm × 200 µm are effectively achieved on PI. After that, another photolithography step can be used to pattern the electrode regions, followed by the Ni metal deposition and lift-off process. Ni is chosen as the electrode material here as it is confirmed to establish ohmic-like contact with InGaSb NWs to ensure a low contact resistance at the NW-metal interface.[22] The device channel is ≈1.5 µm in length with a print density of ≈1 NW µm^{-1} (Figure 2b). Notably, the assembled NW parallel arrays are highly ordered without any significant misalignment, where all NWs are placed with their axis forming an angle less than 5°, with respect to the printing direction. After the flexible photodetector devices are fabricated, they exhibit excellent mechanical robustness. They can be easily bent to any
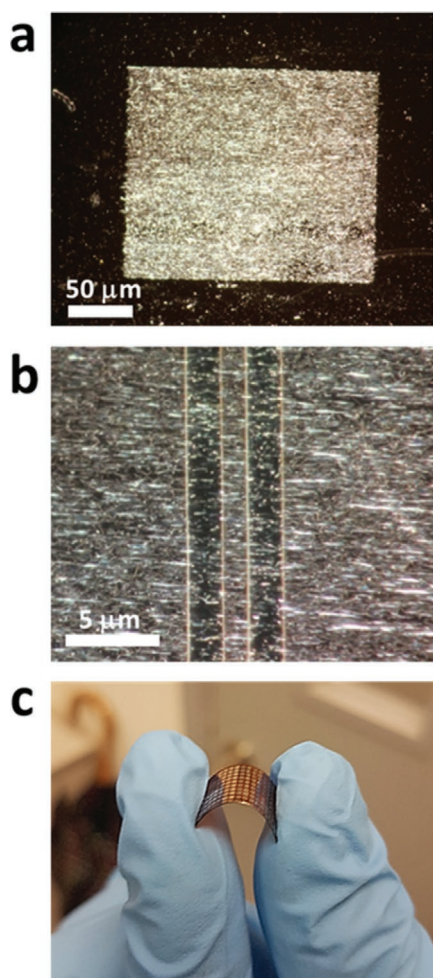
**ADVANCED
SCIENCE NEWS**

www.advancedsciencenews.com

**ADVANCED
OPTICAL
MATERIALS**

www.advopticalmat.de

Figure 2. a) Dark-field optical image of assembled NW parallel arrays on plastics. b) Dark-field optical image of a typical flexible NW parallel-array photodetector illustrating the region of the device channel. c) Optical image of fabricated NW photodetectors under arbitrary mechanical bending.

radius of curvature without any observable delamination and cracking of the metal electrodes (Figure 2c). The thorough electrical characterization and mechanical stability testing of these flexible devices will be presented in the subsequent section.

To shed light on the fundamental properties of flexible NW photodetectors, the typical current–voltage (I–V) measurement of an individual $In_xGa_{1-x}Sb$ NW device with and without the illumination of 1550nm laser (light intensity = 0.71 mW mm^{-2}) is first performed and compiled in Figure S4, Supporting Information. It is worth mentioning that although there is no applied gate bias voltage (i.e., V_{gs} = 0 V), the device still delivers an obvious photoresponse with a source-drain bias voltage (V_{ds}) of 2 V under the photoconductive mechanism (Figure S4d, Supporting Information). This simple photodetector structure does not utilize any complicated p–n junction and related manufacturing techniques; therefore, it can provide versatile device geometry and processing scheme, being ideal for flexible optoelectronics. Once the NW parallel arrays are employed as the device channel, the output current can be effectively scaled up with the number of NWs bridging the metal electrodes

(**Figure 3**a). In general, the photocurrent (I_p) is defined as the difference between the current measured with and without the illumination. The photocurrent is then plotted as a function of light power density in Figure 3b, where there is a nearly linear dependent relationship observed. The curve can be fitted by using an analytical expression of the following:

$$I_p = A\Phi^\beta \tag{1}$$

where A and β are the fitting parameters and Φ is the light intensity. In this case, the β parameter is determined to be 0.647. This sub-linear relationship between the photocurrent and the light intensity is commonly observed in semiconductor-based photodetectors owing to the complex carrier charge transport processes, such electron-hole generation, trapping and recombination.[28] Importantly, this β value is comparable to that obtained from the NW devices fabricated on silicon substrates,[22] indicating that the assembled NW parallel arrays on plastics do not induce any adverse effect on the photoresponse properties of $In_{0.28}Ga_{0.72}Sb$ NWs. At the same time, responsivity is another important figure-of-merit to assess the photodetector performance. It is widely used to evaluate the sensitivity of a photodetector to incident light. It is defined by the ratio of the photocurrent and the light intensity of the incident wavelength, in which it can be described by the following expression:

$$R = \frac{I_p}{\Phi} \tag{2}$$

In other words, it is a description of the conversion efficiency of incident photon into electrical current. Combining Equation (1) and (2), R is proportional to $\Phi^{\beta-1}$. Since the β value of the NW parallel-array device is less than 1, it is expected to have the responsivity decrease with the increasing illumination intensity. This decreasing responsivity is possibly attributed to the trap-assisted photogain mechanism: with a weak light intensity, most of the traps for electrons are not filled, leading to a long lifetime of photo-generated holes, that is, a large photogain; with a strong light intensity, most of the electron traps are filled, leading to a short lifetime of photo-generated holes, that is, a small photogain. As illustrated in Figure 3b, the typical flexible NW photodetector shows an impressive responsivity of 1520 A W^{-1} for the illumination intensity of 0.02 mW mm^{-2} with a V_{ds} of 2 V. This high responsivity value is related to excellent crystallinity of the NW materials. Although this responsivity value is slightly lower than those of the devices fabricated on silicon, it is already the best among all flexible NIR photodetectors recently reported (**Table 1**). This slightly reduced responsibility can be associated with the assembly of NW parallel arrays on plastics, as compared with the ones on silicon, such that the charge traps existing at the NW/plastic interface would act as carrier scattering centers to deteriorate the transport and recombination probability of photo-generated carriers, reducing the photoresponsivity. Better interface passivation schemes are anticipated to decrease the trap concentration there to further improve the detector responsivity.

Apart from the photoresponsivity, the transient response of fabricated flexible photodetectors is also examined to assess their operation stability and response time. To be explicit, the
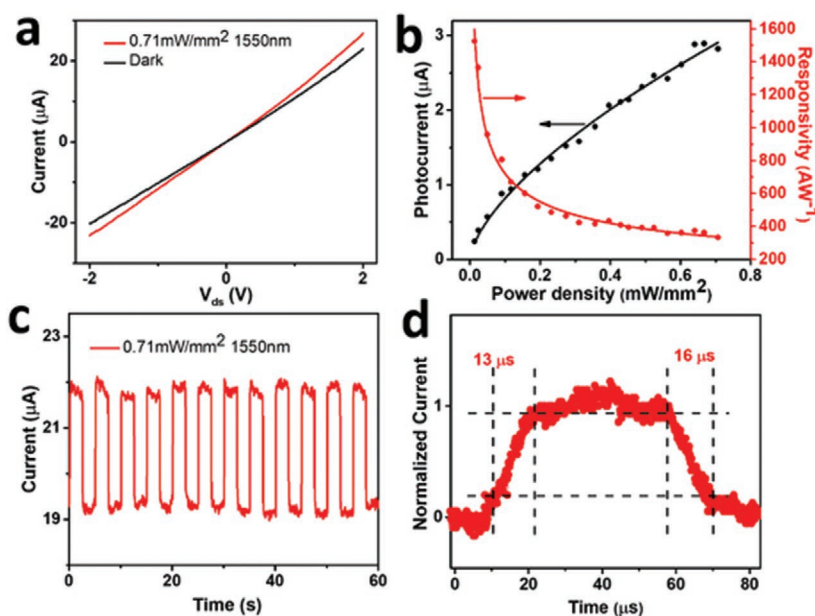
ADVANCED
SCIENCE NEWS
www.advancedsciencenews.com

ADVANCED
OPTICAL
MATERIALS
www.advopticalmat.de

Figure 3. a) Current–Voltage characteristics of a typical flexible NW photodetector with and without the light illumination. b) Photocurrent and responsivity of the detector measured as a function of incident light intensity. c) Photoresponse of the detector under the illumination intensity of 7.1 mW mm^{-2}. d) A high-resolution photoresponse of the detector to demonstrate the rise time and decay time constants. The illumination light source is 1550 nm wavelength. The gate bias is 0 V and the source-drain bias is 2 V for all measurement.

devices are measured under the illumination of 1550 nm light with an intensity of 0.71 mW mm^{-2} and a V_{ds} of 2V with a built-in chopper to manipulate the illumination periodically. It is obvious that when the illumination is turned on, the photocurrent increases rapidly and vice versa. The photocurrent and dark current are measured to be about 22 and 19 μA, respectively. The measurement of twelve different illumination on-off cycles of a typical device is shown in Figure 3c, where the on- and off-current values remain very stable. It is noted that this dark current is relatively high as compared with that of the devices fabricated on silicon because there is no gate layer and gate bias applied in the current flexible device structure; however, the transient photoresponse of our devices is highly repeatable, being sufficient for flexible optoelectronic applications without utilizing complicated device fabrication schemes. On the other hand, the response times (i.e., rise time and decay time) of photodetectors are also critical for practical utilization. Figure 3d depicts a high-resolution transient photoresponse of the flexible detector to evaluate the rise time and decay time constants. Generally, the rise (decay) time constant is defined by the time required for the current to increase from 10 to 90% (to decrease from

90 to 10%) of the peak value. In this work, a photoresponse measurement circuit is designed and employed to examine these response speeds, where the rise and decay time constants are found to be 13 and 16 μs, respectively, indicating the ultrafast response of our devices. To the best of our knowledge, even without using any p–n junctions, these efficient responses constitute a record low value of response time among all flexible NIR photodetectors (Table 1). Typically, the response speed of a photoconductive detector is related to the lifetime of photo-generated carriers (τ) and trap density with trapped charges (p_t) in a way of $t = (1 + p_t/p)\tau$, where t is the response time and p is the hole concentration. This fast response speed indicates the short lifetime and low density of charge traps here. It is also worth noting that this response speed of NW parallel-array devices is actually very similar to that of individual NW devices (Figure S4f, Supporting Information), which suggest again that the assembly of NW parallel arrays on plastics does not degrade the fundamental photoresponse properties of individual NWs, attributable to the growth of highly-crystalline, phase- and orientation-pure $In_{0.28}Ga_{0.72}Sb$ NWs as well as the reliable NW printing for the establishment of uniform NW parallel

Table 1. Performance comparison among flexible NIR photodetectors reported in the recent literature.

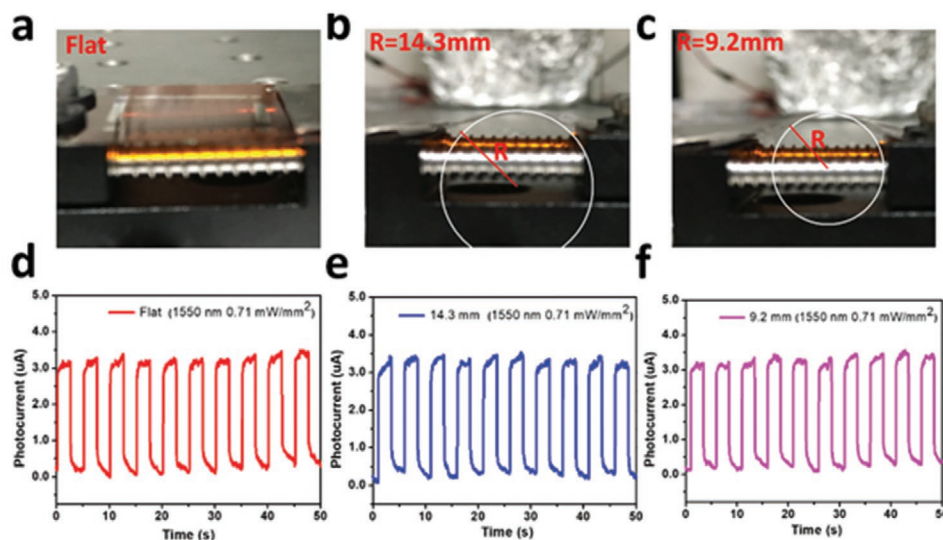| Channel materials	Incident wavelength [nm]	Responsivity [A W^{-1}]	Bias voltage [V]	Operating temperature	Rise time/decay time	Ref.
p-Si/n-CdS NW	1550	6.2×10^{-6}	N/A	RT	1.47/1.37 ms	[29]
MoSe$_2$	1550	2.6	0.05	RT	3.9/2.9 s	[6]
SnTe	1550	10.91	1	RT	N/A	[7]
Graphene/AuOx	1550	9	0.1	RT	N/A	[30]
Quasi-1D NbS$_3$	1550	N/A	N/A	RT	4.71 ms	[31]
InGaSb NW arrays	1550	1520	2	RT	13/16 μs	This work

Figure 4. a–c) Optical images of measurement setup of the device with different bending conditions for the evaluation of mechanical stability. d–f) Photoresponse of the flexible NW parallel-array photodetector with different bending radii of curvature.

arrays. In future, the photodetector performance can be further enhanced by improving the NW print density, optimizing the channel dimension, and so on.

For flexible optoelectronics, the mechanical stability and operation durability of the devices are extremely important for applications. The mechanical robustness of flexible NW parallel-array photodetectors can be evaluated by measuring their photoresponse under different mechanical bending conditions. In particular, the detectors (30 mm × 30 mm in dimension) are first mounted onto a custom-designed holder with a precise control of different bending angles (i.e., different radii of curvature), and then assessed with their photoresponse as a function of time under the illumination of 1550 nm light. **Figure 4**a–c show the optical images of measurement setup with the device lying flat, bending to radii of curvature of 14.3 mm and 9.2 mm, respectively, whereas Figure 4d–f present the corresponding photoresponse of the device. As the bending experienced by different NW array devices varies depending on their location, it is understood that all the devices are not under the said bending curvature. The devices under the maximum bending are measured here. When the device does not receive any bending, it is expected to deliver stable photoresponse

under different illumination on-off cycles as discussed above (Figure 3c). Interestingly, when the device is bent along the NW printing direction with different radii of curvature, it still exhibits the same consistent photoresponse, especially for the stable on- and off-current (i.e., photocurrent and dark current), without any noticeable property degradation. This excellent mechanical stability can be ascribed to the superior flexibility of NW materials, which is in a distinct contrast to other conventional thin film materials used in flexible photodetectors.

In addition, the device durability can be examined by continuously measuring the photoresponse as a function of time with repeated illumination on-off cycles as well as the stability of photocurrent under different bending cycles. For simplicity, the photocurrent here is normalized to that obtained in the case where no mechanical bending is performed. As presented in **Figure 5**a, after 1000 seconds of continuous operation (i.e., 100 rise-and-decay cycles), there is no significant photoresponse degradation witnessed for the device lying flat. Considering that the device is not passivated and protected by any packaging, such operation stability in ambient air condition is respectable. Simultaneously, the device can also be bent repeatedly by using the above-mentioned device holder. The device is first lying flat, bent
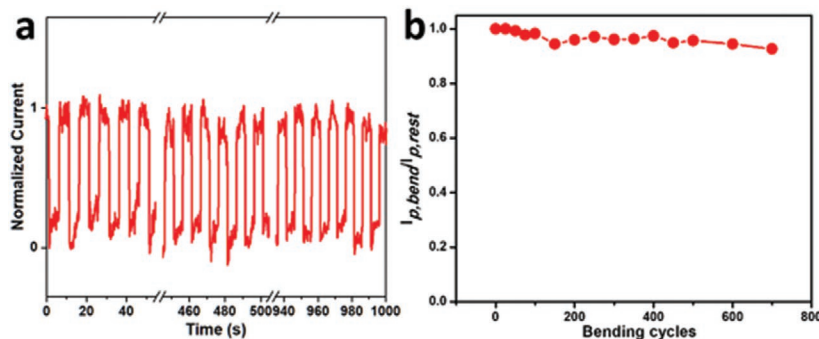

Figure 5. a) Photoresponse stability of flexible NW parallel-array photodetectors as a function of time with different illumination on-off cycles under 1550 nm wavelength. b) Photocurrent of the flexible detector as a function of different mechanical bending cycles.

with the radius of curvature down to 9.2 mm and then recovered back to the flat condition for each bending cycle. It is impressive that the device only exhibits an insignificant degradation (only 7% decrease) in the photocurrent after 700 bending cycles (Figure 5b). The excellent bending endurance can be attributed to the excellent flexibility of the NWs. The slight photocurrent reduction is possibly related to degradation of the electrical contact between metal electrodes and NW channels as well as the NW fracture in the channel. This way, device encapsulation may be essential to enhance the electrical contact for the device durability improvement. In any case, all these results indicate the promising potential of these $In_{0.28}Ga_{0.72}Sb$ NW parallel arrays for high-performance flexible thin-film NIR photodetectors.

In summary, we have successfully grown high-quality $In_{0.28}Ga_{0.72}Sb$ NWs with the two-step CVD method and assembled high-density regular NW parallel arrays on PI substrates. When they are configured into photodetectors, they display excellent photoresponsivity up to 1520 A W^{-1} and ultrafast response speed below 20 µs toward 1550 nm irradiation at room temperature, constituting a record high performance among all flexible NIR photodetectors reported in recent literature. More importantly, these flexible photodetectors also exhibit outstanding mechanical stability and operation durability. They can provide very stable photoresponse with illumination on-off cycles up to 1000 s. After they are measured with 700 bending cycles, they only give an insignificant degradation in their photocurrent. All these findings evidently illustrate the impressive device performance and promising prospect of our large-scale InGaSb NW arrays for practical applications in next-generation high-performance flexible optoelectronics.

3. Experimental Section

Synthesis and Characterization of Nanowires: The detailed synthesis procedures of $In_xGa_{1-x}Sb$ NWs were reported elsewhere.[22] In brief, the entire growth process was performed in a two-heating zone horizontal furnace with a quartz tube of one inch in diameter. Si/SiO$_2$ (50 nm thick thermal oxide) wafer pieces were utilized as the growth substrates. They were first coated with an Au thin film (0.1 nm in the nominal thickness) by thermal evaporation as the catalyst. Then, they were placed in the center of the downstream zone. The powder mixture of InSb and GaSb was used as the precursor source. The composition of the NWs could be simply controlled by varying the precursor powder mixing ratio. For example, 1 g of source powder (InSb: GaSb = 40:1 in weight %) was loaded into a boron nitride crucible positioned in the center of the upstream zone to grow the $In_{0.28}Ga_{0.72}Sb$ NWs. During the growth, the pressure of the system was pumped down to a baseline pressure of 1.5×10^{-3} Torr by a mechanical pump. 100 sccm H$_2$ was introduced as the carrier gas to achieve the process pressure of 2.1 Torr. Both upstream and downstream zones were heated to 750 and 510 °C, respectively, in 10 min, which were maintained at these temperatures for 180 min for the NW synthesis. After that, the furnace was cooled down to room temperature. The morphologies of the grown NWs were examined by a field-emission scanning electron microscope (SEM, XL30, Philips, Netherlands). For the transmission electron microscope (TEM, CM-20, Philips, Netherlands), high-resolution TEM (JEOL 2100F, JEOL Co., Ltd., Japan) and elemental mapping studies, the NWs were first suspended in anhydrous ethanol solution by ultra-sonication and then drop-casted onto the TEM grid for the corresponding characterization.

Photodetector Fabrication: To fabricate the NW parallel-array thin-film photodetectors, the grown $In_{0.28}Ga_{0.72}Sb$ NWs were first assembled into large-scale, high-density, and regular parallel arrays on PI substrates

(0.2 mm in thickness) by using the well-developed contact printing technique.[25–27] During the NW printing, the donor NW chip (i.e., the growth substrate with NWs) was flipped onto and then slid against the target chip (i.e., the PI substrate with pre-defined NW receiving region by photolithography supported on Si/SiO$_2$ pieces) at a rate of 10 mm min^{-1} with a constant pressure of 50 g cm^{-2}. This way, the $In_{0.28}Ga_{0.72}Sb$ NW parallel-array thin films were successfully printed onto the patterned region after photoresist removal. Next, another step of photolithography was employed to define the electrode regions, followed by a thermal deposition of a 100 nm-thick Ni film and a lift-off process.

Photodetector Characterization: After the fabrication of flexible NW photodetectors, their device performance was carefully characterized in a standard probe station together with an Agilent 4155C semiconductor analyzer (Santa Clara, CA, USA). A 1550nm laser, with a built-in modulator (AFG 2005, Arbitrary Function Generator, Good Will Instrument Co. Ltd), was used as the excitation light source with the capability to modulate the light and to tune the power of the light, respectively. A low-noise current amplifier (SR570, Stanford Research Systems, USA) combined with a digital oscillator (TBS 1102B EDU, Tektronix, USA) was used to obtain the high-resolution current versus time curves to determine the response time of fabricated photodetectors. The detailed measurement setup can be seen in Figure S5, Supporting Information. The intrinsic speed of the measurement system was evaluated by using a commercial InGaAs photodiode (FDGA05, Thorlabs) in order to ensure the accurate determination of the response speed of fabricated photodetectors. The intrinsic rise and decay times of the system were measured to be 0.65 and 1.96 µs, respectively (Figure S6, Supporting Information), which are shorter than those of NW devices, indicating the validity of the measurement results. All measurements were done under ambient conditions without any active cooling of the devices.

Supporting Information

Supporting Information is available from the Wiley Online Library or from the author.

Acknowledgements

Conflict of Interest

The authors declare no conflict of interest.

Keywords

[1] W. Gao, H. Ota, D. Kiriya, K. Takei, A. Javey, *Acc. Chem. Res.* **2019**, *52*, 523.

[2] Y. Liu, M. Pharr, G. A. Salvatore, *ACS Nano* **2017**, *11*, 9614.

[3] Y. Li, G. Xu, C. Cui, Y. Li, *Adv. Energy Mater.* **2018**, *8*, 1701791.

[4] X. Wang, L. Dong, H. Zhang, R. Yu, C. Pan, Z. L. Wang, *Adv. Sci.* **2015**, *2*, 1500169.

[5] A. Chortos, J. Liu, Z. Bao, *Nat. Mater.* **2016**, *15*, 937.

[6] V. Dhyani, P. Kumari, S. Maity, S. Das, *Proc. SPIE* **2019**, *11028*, 110282G.

[7] J. Yang, W. Yu, Z. Pan, Q. Yu, Q. Yin, L. Guo, Y. Zhao, T. Sun, Q. Bao, K. Zhang, *Small* **2018**, *14*, 1802598.

[8] H. Kim, J.-H. An, *Carbon* **2017**, *120*, 244.

[9] Y. Sun, J. A. Rogers, *Adv. Mater.* **2007**, *19*, 1897.

[10] Z. Liu, J. Xu, D. Chen, G. Shen, *Chem. Soc. Rev.* **2015**, *44*, 161.

[11] X. Liu, Y.-Z. Long, L. Liao, X. Duan, Z. Fan, *ACS Nano* **2012**, *6*, 1888.

[12] M. Beeler, E. Trichas, E. Monroy, *Semicond. Sci. Technol.* **2013**, *28*, 074022.

[13] L. Shen, E. Y. B. Pun, J. C. Ho, *Mater. Chem. Front.* **2017**, *1*, 630.

[14] N. Han, Z. Yang, F. Wang, G. Dong, S. Yip, X. Liang, T. F. Hung, Y. Chen, J. C. Ho, *ACS Appl. Mater. Interfaces* **2015**, *7*, 20454.

[15] N. Guo, W. Hu, L. Liao, S. Yip, J. C. Ho, J. Miao, Z. Zhang, J. Zou, T. Jiang, S. Wu, X. Chen, W. Lu, *Adv. Mater.* **2014**, *26*, 8232.

[16] a) J. Miao, W. Hu, N. Guo, Z. Lu, X. Zou, L. Liao, S. Shi, P. Chen, Z. Fan, J. C. Ho, T.-X. Li, X. S. Chen, W. Lu, *ACS Nano* **2014**, *8*, 3628; b) H. Tan, C. Fan, L. Ma, X. Zhang, P. Fan, Y. Yang, W. Hu, H. Zhou, X. Zhuang, X. Zhu, A. Pan, *Nano-Micro Lett.* **2016**, *8*, 29.

[17] H. Li, H. Alradhi, Z. Jin, E. A. Anyebe, A. M. Sanchez, W. M. Linhart, R. Kudrawiec, H. Fang, Z. Wang, W. Hu, Q. Zhuang, *Adv. Funct. Mater.* **2018**, *28*, 1705382.

[18] T. Duan, C. Liao, T. Chen, N. Yu, Y. Liu, H. Yin, Z.-J. Xiong, M.-Q. Zhu, *Nano Energy* **2015**, *15*, 293.

[19] L. Ma, W. Hu, Q. Zhang, P. Ren, X. Zhuang, H. Zhou, J. Xu, H. Li, Z. Shan, X. Wang, L. Liao, H. Q. Xu, A. Pan, *Nano Lett.* **2014**, *14*, 694.

[20] Q. Li, S. Wang, Y. Chen, M. Yan, L. Tong, M. Qiu, *IEEE J. Sel. Top. Quantum Electron.* **2011**, *17*, 1107.

[21] S. Yip, L. Shen, J. C. Ho, *Nanotechnology* **2019**, *30*, 202003.

[22] D. Li, C. Lan, A. Manikandan, S. Yip, Z. Zhou, X. Liang, L. Shu, Y.-L. Chueh, N. Han, J. C. Ho, *Nat. Commun.* **2019**, *10*, 1664.

[23] L. Ma, X. Zhang, H. Li, H. Tan, Y. Yang, Y. Xu, W. Hu, X. Zhu, X. Zhuang, A. Pan, *Semicond. Sci. Technol.* **2015**, *30*, 105033.

[24] Z. Li, X. Yuan, L. Fu, K. Peng, F. Wang, X. Fu, P. Caroff, T. P. White, H. Hoe Tan, C. Jagadish, *Nanotechnology* **2015**, *26*, 445202.

[25] Z. Fan, J. C. Ho, Z. A. Jacobson, R. Yerushalmi, R. L. Alley, H. Razavi, A. Javey, *Nano Lett.* **2008**, *8*, 20.

[26] A. C. Ford, J. C. Ho, Z. Y. Fan, O. Ergen, V. Altoe, S. Aloni, H. Razavi, A. Javey, *Nano Res.* **2008**, *1*, 32.

[27] T. Takahashi, K. Takei, J. C. Ho, Y. L. Chueh, Z. Y. Fan, A. Javey, *J. Am. Chem. Soc.* **2009**, *131*, 2102.

[28] a) B. E. A. Saleh, M. C. Teich, *Fundamentals of Photonics*, Wiley, New York **2013**; b) C. Lan, C. Li, S. Wang, T. He, Z. Zhou, D. Wei, H. Guo, H. Yang, Y. Liu, *J. Mater. Chem. C* **2017**, *5*, 1494.

[29] Y. Dai, X. Wang, W. Peng, C. Xu, C. Wu, K. Dong, R. Liu, Z. L. Wang, *Adv. Mater.* **2018**, *30*, 1705893.

[30] Y.-L. Liu, C.-C. Yu, K.-T. Lin, T.-C. Yang, E.-Y. Wang, H.-L. Chen, L.-C. Chen, K.-H. Chen, *ACS Nano* **2015**, *9*, 5093.

[31] W. Wu, Y. Wang, Y. Niu, P. Wang, M. Chen, J. Sun, N. Wang, D. Wu, Z. Zhao, *ACS Appl. Mater. Interfaces* **2020**, *12*, 14165.